Pastor, JV.; García Martínez, A.; Mico Reche, C.; De Vargas Lewiski, F. (2020). An optical investigation of Fischer-Tropsch diesel and Oxymethylene dimethyl ether impact on combustion process for CI engines. Applied Energy. 260:1-12. https://doi.org/10.1016/j.apenergy.2019.114238

An optical investigation of Fischer-Tropsch diesel and Oxymethylene Dimethyl Ether impact on combustion process for CI Engines

José V. Pastor, Antonio García, Carlos Micó, Felipe Lewiski

CMT - Motores Térmicos, Universitat Politècnica de València, Camino de Vera s/n, 46022 Valencia, Spain

Corresponding author (*): Carlos Micó

e-mail: carmirec@mot.upv.es

Phone: +34 654919619

Abstract

Synthetic fuels (E-fuels) have shown to be an interesting alternative to replace the fossil diesel fuel due to its CO_2 reduction potential as well as for their capability to diminish the soot production and therefore for improving the soot-NO_X trade-off in Compression Ignition engines. Thus, the main objective of this paper was to better understand the combustion process and the in-cylinder soot formation of two of the most popular E-fuels currently: Fischer-Tropsch (FT) diesel and Oxymethylene dimethyl ether (OME_X). To achieve this aim, a single cylinder optical CI engine with a commercial piston geometry was used. Thee optical techniques (Natural Luminosity–NL, OH* chemiluminescence and 2-color pyrometry) were applied to analyze the combustion evolution and quantify the soot formation at different loads (1.5, 4.5 and 7.5 bar IMEP). OME_X presented the largest injection duration due to the low LHV. For the NL analysis, OME_X showed the lowest light intensity for the three loads tested, indicating a very low soot production. Despite of the low NL intensity, it presented the highest OH* chemiluminescence signal, indicating a higher presence of near-stoichiometric zones due to the high amount of oxygen. Regarding FT diesel, it showed a combustion behavior similar to the commercial diesel. NL, OH* and 2-color technique analysis indicated that

for the three conditions tested, FT diesel presented lower soot production and a faster soot oxidation than commercial diesel.

Keywords

E-fuels; soot reduction; OME_X; FT diesel; Oxygenated fuels; Optical engines; Optical Techniques

1. Introduction

The continuous increase of energy demand as well as the strict emissions legislation have forced the automotive industry to seek for innovative and more efficient solutions, in terms of internal combustion engine technologies. Regarding compression ignition engines, which are known for its high thermal efficiency, the biggest challenge has been reducing the soot particles and NO_X emissions.

Alternative fuels, new combustion concepts such as dual fuel[1–3] and partially premixed[4,5] or new hardware designs[6,7] are being studied and applied in order to obtain more efficient and less-pollutants engines. Synthetic fuels (E-fuels) have shown to be a suitable solution for both reducing harmful emissions and the fossil fuel dependence[8]. They can be both gaseous or liquid fuels, which are generated from renewable electricity in a synthetic process[9] consuming carbon dioxide and water. Thus, it is considered a carbon-neutral fuel.

Among these so called E-fuels, Fischer-Tropsch (FT) diesel can be considered an interesting alternative to replace the fossil diesel. FT diesel, which is composed by different n-alkanes molecules, can be obtained from different natural resources e.g. biomass [10]. This fuel has similar properties as fossil diesel such as viscosity, lubricity, cold-flow properties, flash temperatures and boiling temperature, covering all required

diesel specifications. In relation to the spray behavior, an analysis of the liquid length and vapor penetration of Fischer-Tropsch was developed by Kook and Picket [11] based on the use of Schlieren and Mie-scattering techniques in a constant-volume chamber. Results showed longest liquid length for the diesel in comparison with Fischer-Tropsch and no significant differences for the vapor penetration, which means an improvement of air-fuel mixing. Taking into account that FT diesel does not contain neither sulfur nor aromatics and it has a high cetane number, the results related with the pollutant emissions reduction are very positive[12,13]. By using this kind of fuel, different studies have demonstrated a reduction of PM, CO and HC emissions [12,14,15] but different results were obtained for the NO_X emissions. Jiao et al[16] studied the emissions of a methanol-Fischer Tropsch diesel-biodiesel-diesel blends in comparison with fossil diesel at different altitudes. Results demonstrated that blends reduced the PM emissions for all altitudes tested while the NO_X emissions were slightly higher, showing similar behavior to the typical NO_X/soot trade-off present in the fossil diesel combustion. In this case, it is important to highlight the increasing of NO_X could be the effect of any of the three fuels used in the blend. In addition, the non-use of EGR contributed to this effect. In contrast, Rimkus et al [12] analyzed the emissions from a diesel/FT diesel blend with 15% of the synthetic component in a high speed turbocharged CI engine. The results indicated that, in comparison with fossil diesel, HC emissions were reduced by 3-7%, soot reduced by 16-18% and NO_X reduced by 9-12%. Furthermore, other studies have reported an improvement in the well-known NOx and soot trade-off in compression ignition engines by using adequate blending and EGR [14,17,18]. Schaberg et al [19] analyzed the Fischer-Tropsch combustion in an optical diesel engine by means of OH* chemiluminescence and two color spectroscopy. The authors reported a reduction of

soot radiation for the Fischer-Tropsch in comparison with diesel. Regarding the thermal efficiency and brake specific fuel consumption, Gill et al [15]reported a compilation of several publications that have studied the FT diesel in comparison with the fossil diesel. The major percentage of publications have reported higher thermal efficiency and lower brake specific fuel consumption for the FT diesel.

Another interesting E-fuel family is the oxymethylene dimethyl ethers (OME_X), which are formed by a CH_3-O-(CH_2-O)$_x$-CH_3 chemical structure being x in the range of 1 to 5 [20]. This fuel can be produced by using methanol and formaldehyde[21]. Considering the high amount of oxygen atoms and the absence of any C-C bonds, the OME_X combustion process is practically free of soot emission. OME1 is the simplest chemical structure of the OME_X, but it presents storage and handling problems due to the very low boiling point. In this way, it is necessary to modify the fuel injection system to avoid vapor lock problems [20,21]. In addition, because of the low cetane number (CN30)[22] and viscosity, chemical structures of OME_X with longer chains (x=3,4,5) are considered more interesting as they contain properties more similar to fossil diesel [23]. By increasing the chain length of OME_X, the cetane number, lubricity and flash point are significantly improved, while increasing the O/H ratio and the capacity of soot reduction. However, OME_X structures with X≥5 present problems with cold-flow properties [13]. Regarding emissions, different studies have provided good results in terms of soot, HC and CO emissions reduction[24][25]. Omari et al [8] have studied the emissions for the pure OME_{3-5} and blends with diesel fuel in a single cylinder diesel engine. For all the blends and fuels tested, the CO, HC and PM emissions were lower than the ones corresponding to the fossil diesel. In addition, the PM emission for the case of pure OME_{3-5} was almost zero. Some optical investigations about the soot formation [20][26] have been

performed in constant volume vessels with different blends of OME_X and diesel. Ianuzzi et al [20] reported a massive reduction of the soot formation when increasing the oxygenated fraction (OME_X) in the blend. Ma et al [26] have found a soot emission reduction of 68% by using blends with up to 30% OME_X and without the necessity of any modification in the engine combustion control strategies. However, in terms of NOx emissions, different results can be found in the literature. Liu et al[27] reported an increase of NOx emissions as the OME_{3-4} quantity was increased in the OME_{3-4}/diesel blend. However, contrary to this, Lump et al. [28] found that the NOx emissions decreased with the addition of 20% of OME_{3-4}. Considering the high amount of oxygen in the fuel, some authors have reported the possibility of reducing the NO_X emissions by using high EGR rates without increasing the soot and PM emissions [21,23]. Due to the low lower heating value (LHV), the specific fuel consumption for the OME_X increases[27]. Furthermore, because its density is higher than fossil diesel, the amount of fuel injected is different for the same energizing time (ET) and injection pressure[21], resulting in different injection strategies. However, despite requiring longer injection durations than fossil diesel for the same IMEP due to lower LHV, the combustion duration is shorter which results in a higher thermodynamic efficiency[23].

Taking into account the potential of E-fuels in order to reduce pollutant emissions, the current work aims to analyze the combustion process and in-cylinder soot formation of the two mentioned E-fuels (FT diesel and OME_X) when they completely replace fossil diesel in a compression ignition (CI) engine. To achieve this goal, a single cylinder optical CI engine with a commercial piston geometry and three different optical techniques have been applied simultaneously in this work. For a qualitative analysis of the soot formation and combustion process evolution, the natural luminosity has been

registered. In addition, OH* chemiluminescence has been used for the identification of high temperature reaction zones where air/fuel ratio is close to the stoichiometric and the OH* in the excited state is present. Finally, the soot formation has been quantified by using the 2-color pyrometry technique. Different loads for each considered fuel have been tested in the optical engine.

The results of this work complement other studies with similar topic based on full-metal engines by providing information regarding in-cylinder soot formation, in comparison to only exhaust soot emission reported by other authors. Additionally, in contrast with most of the research based on optical engines, the use of a realistic bowl geometry (instead if a simple one) allows to be closer to the real operating conditions of commercial engines. Finally, it must be highlighted that no previous studies were found where e-fuels (FT diesel and OME_x) are compared in the same engine.

2. Experimental methodology

2.1. Optical engine

A single-cylinder optical direct injection diesel engine with a piston extension was used to perform the tests. The optical engine is derived from a GM commercial diesel engine with a displacement of 400 cm^3 per cylinder. The original GM cylinder head was assembled in the optical engine. It presents 4 valves per cylinder and a centrally located Denso solenoid injector with 8 holes. Furthermore, bore and stroke were kept the same as the commercial engine. The geometric information is summarized in table 1.

Table 1. Engine characteristics

Engine type	4 stroke, direct injection
Number of cylinders [-]	1
Number of Valves [-]	4
Bore [mm]	80
Stroke [mm]	80.1
Compression ratio [-]	12.5:1
Bowl Type	Re-entrant
Displacement [l]	0.402

The main optical access available is from below of the combustion chamber, by means of a completely transparent quartz piston top. The piston has a real bowl shape in order to mimic as much as possible the flow dynamics and combustion process of the real full-metal engine. The other two optical access are formed by two quartz windows located in the upper part of the liner, one at each side of the engine as shown in figure 1. The piston rings are composed by a synthetic material which expands as the in-cylinder temperature increases, in order to avoid the air leakage (blow-by).

The injection system consists of a common rail and its control is performed electronically by using a DRIVVEN® control unit. This device allows flexibility in terms of injection parameters such as start of energizing (SOE), number of injections per cycle, number of cycles without combustion (skip fire), etc.

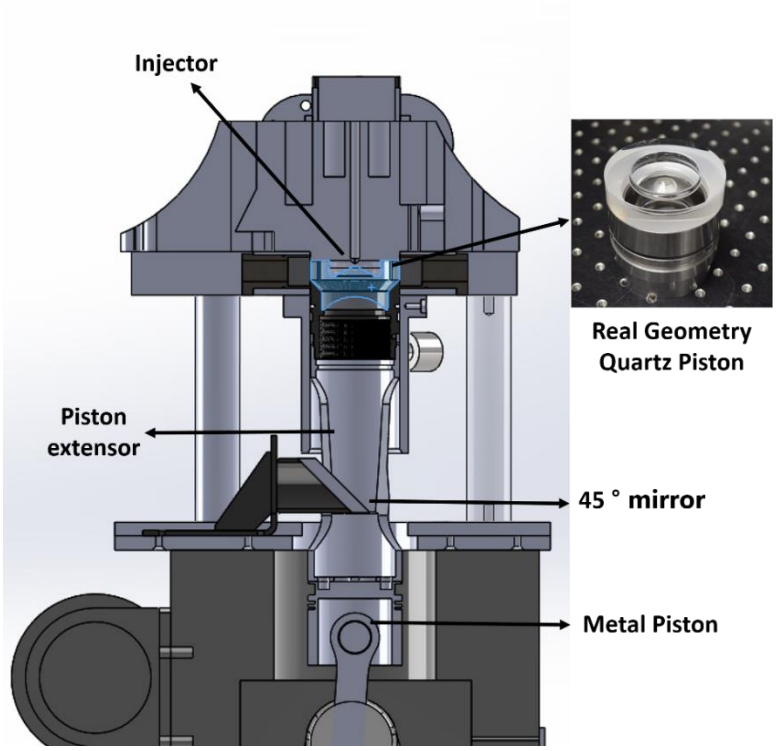

Figure 1. Optical engine assembly

2.2. Test cell

In figure 2 the test cell diagram is shown. It represents all equipment necessary for the engine operation, control and acquisition data. A screw compressor supplies the intake air at the required pressure for each test condition. Besides, a dryer and a heat exchanger is used to achieve the desired temperature and humidity of the intake air. The air heater is located just before the intake port and it provides a constant air temperature. An exhaust backpressure valve is used in order to control the exhaust pressure and to simulate more realistic conditions. The exhaust pressure was always kept 0.2 bar higher than the intake pressure. To avoid pressure pulses in the intake and exhaust lines, a plenum chamber was installed in the test cell.

The optical engine is connected to an electric dynamometer, which allows controlling the load and engine speed. The in-cylinder pressure was measured with an AVL GH13P

glow-plug piezoelectric transductor coupled to a Kistler 4603B10 charge amplifier. The pressure signal was measured by a Yokogawa DL708E oscillographic recorder with a 16 bits A/D converter module. A shaft encoder with 1800 pulses per revolution, which allows a 0.2 CAD resolution was used in order to synchronize the acquisition system. The mean variables such as intake air temperature, intake air pressure and cooling water temperature were acquired at a low sampling frequency of 100 Hz using SAMARUC, a home-developed test system that collects the signals of different sensors and controls the electric dynamometer. Table 2 shows the accuracy of the different elements of the test cell. The injector drive signal was obtained by using a current impulse Kistler sensor. This signal also was monitored using a Yokogawa DL 708E.

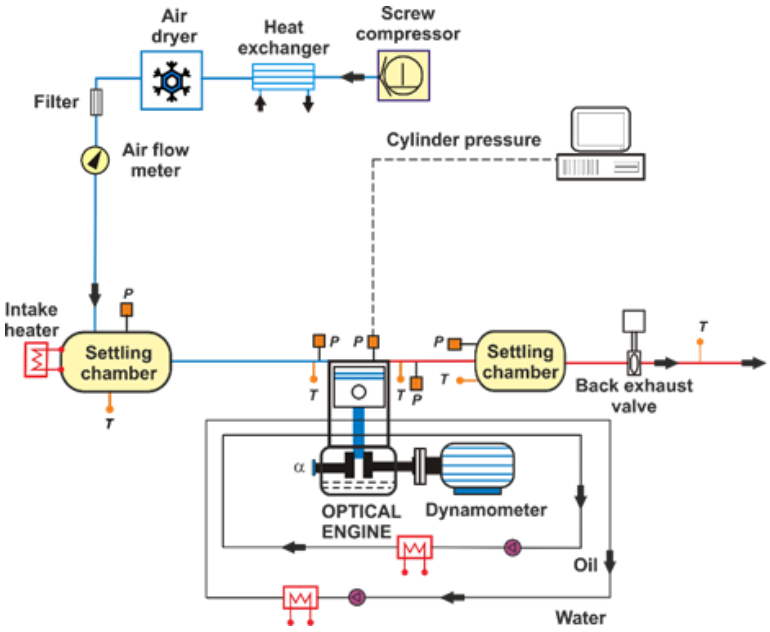

Figure 2. Test cell scheme

Table 2. Information of measurement instruments

Variable	Device	Manufacturer / model	Accuracy
In-cylinder pressure	Piezoelectric transducer	AVL / GH13P	±1.25 bar
Intake/exhaust pressure	Piezorresistive transducers	Kistler / 4603B10	±25 mbar
Temperature in settling chambers and manifolds	Thermocouple	TC direct / type K	±2.5 °C
Crank angle, engine speed	Encoder	AVL / 364	±0.02 CAD
Air mass flow	Air flow meter	Sensyflow / FTM700-P	< ±1%

2.3. Fuels

The main properties of the fuels studied in this work are presented in the table 3. Commercial diesel (EN 590 diesel) was considered the reference fuel in the study. Fischer-Tropsch (FT) diesel and Oxymethylene ether (OME_X) were used without mixing. Cetane number for FT diesel and OME_X is clearly higher than for the commercial diesel, indicating that their ignitability is higher[29]. OME_X presents the lowest viscosity between the three tested fuels, which directly implies in an improvement of the spray quality[30]. Finally, regarding the Lower Heating Value (LHV), FT diesel and commercial diesel have very similar values. However, OME_X's LHV is less than the half of the commercial diesel's. This has a direct impact in fuel consumption.

Table 3. Fuel properties

	EN 590 diesel	FT diesel	OME_X
Density [kg/m^3] (T= 15 °C)	842	832	1067
Viscosity [mm^2/s] (T= 40 °C)	2.929	3.25	1.18
Cetane number [-]	55.7	75.5	72.9
Carbon content [% m/m]	86.2	85.7	43.6
Hydrogen content [% m/m]	13.8	14.3	8.82
Oxygen content [% m/m]	0	0	47.1
Lower heating value [MJ/kg]	42.44	44.2	19.04

2.4. Operating conditions

For all tests, engine speed was fixed at 1200 rpm for three different IMEP (1.5, 4.5 and 7.5 bar). For each load, different intake pressures and temperatures were used, which are presented in the table 4. The exhaust pressure was always kept 0.2 bar higher than the intake pressure. Oil temperature is kept constant at 60 °C. Furthermore, the coolant temperature varies between 15 °C and 25 °C in order to preserve the piston rings and optical accesses.

Table 4. Engine conditions

Inj. Pattern	Engine Speed	IMEP (bar)	Pint (Bar)	Tint (°C)	Toil (°C)	Tcool (°C).
Mult.	1250	1.5	1.5	100	60	15-25
		4.5	1.9	90		
		7.5	2.15	90		

The injection strategy is the same used for the calibration of the metal version of the engine as reported in [31]. The injection strategy has 4 injection events with 2 pilots, a main and a post injection. The same strategy have been used by different authors [32][33][34] in order to reduce the NO_X and soot emissions as well as improve the performance at cold start conditions. For each IMEP tested, a different injection pressure (800, 670 and 400 bar) was used. Considering the different LHV and cetane number of each fuel, the injection timing and injection duration were adjusted in order to keep the same IMEP and similar CA50. To preserve the optical access and the piston rings, the optical engine was operated in a skip fire mode with one combustion cycle every twenty cycles. The injection timings used for each engine load and fuels is represented in the table 5:

Table 5. Injection timings

Fuel	IMEP [bar]	Inj. Pressure [bar]	Injection timing [CAD]			
-	-	-	Pilot 1	Pilot 2	Main	Post
diesel	1.5	400	-14.65	6.36	-2.2	4.46
	4.5	670	-14.1	6.36	-2.2	7
	7.5	800	-16.55	-6.36	-2.2	8.06
TP diesel	1.5	400	-13.5	-6.15	-2.2	3.825
	4.5	670	-13.44	-6.7	-2.2	6.7
	7.5	800	-15.45	-6.66	-2.2	7.95
OME_X	1.5	400	-13.5	-6.15	-2.2	6.825
	4.5	670	13.44	-6.7	-2.2	9.18
	7.5	800	-15.45	-6-68	-2.2	10.5

2.5. Optical Techniques

For the current work, three optical techniques have been applied simultaneously in order to identify and analyze the differences in the combustion process for each fuel tested. The optical setup is presented in figure 3.They were positioned in order to record the flame radiation that comes from the main optical access (piston bottom). A 45° mirror is positioned just below the piston in order to reflect all flame radiation from the combustion chamber to the optical system. A dichroic mirror was used to reflect the UV radiation to the intensified camera (ICCD), which was positioned 90° relative to the engine's crankshaft. After the dichroic mirror, which is transparent for the visible range (up to 750nm), a beam splitter was positioned to separate flame radiation between two high speed cameras (550nm and 660 nm). One of them was equipped with a 660 nm filter, which is used for both 2-color measurements as well as for the natural luminosity

imaging. The other one was equipped with a 550 nm filter, which was used for 2-color pyrometry.

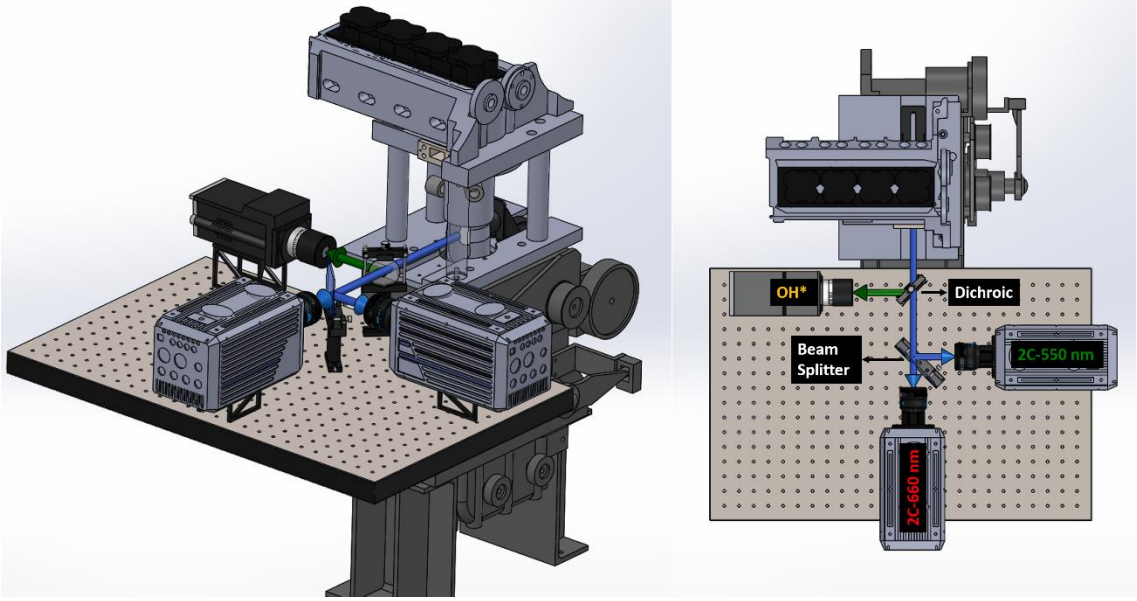

Figure 3. Optical set up

2.5.1. High-Speed Soot Natural Luminosity Imaging

The Natural luminosity (NL) images have been used in order to provide general information about the combustion process evolution. They correspond to hot soot radiation, which is the dominant source of luminosity in diffusive combustion[35]. However, interpretation of NL images has to be done carefully because there are many factors that affect the NL signal such as soot particle temperature, size and optical properties [36]. High light intensity in a NL image could come from high temperature areas, high soot concentration areas, or a combination of both of them. In this way, NL images provide only qualitative information regarding the combustion evolution, late-cycle oxidation, etc. However, it is not possible to quantify the soot volume fraction generated during the combustion process.

For the NL measurements a Photron SA-5 high speed CMOS camera was used. Due to differences in flame radiation, exposure time was set to 6.65 μs for commercial diesel and FT diesel while 35.5 μs was set for the OME_X fuel. The image resolution was kept at 512 x 512 pixels with a spatial resolution of 8.1 pixels/mm. Taking into account the image resolution used for the tests, the maximum frame rate allowed was 25 kfps. 6 repetitions were recorded for each condition tested.

2.5.2. OH* chemiluminescence

The OH* chemiluminescence signal was used in the present work in order to identify the near-stoichiometric high temperature combustion zones inside the piston. This zones are characterized for high concentration of excited-state OH*. Considering that soot natural luminosity is formed in zones with rich combustion, the combination of this signal with OH* radiation helps to get more information about the combustion process [37]. For the stoichiometric zones inside the bowl, where OH* is formed, the soot oxidation is promoted easily. However, in the rich zones the only way to guarantee the soot oxidation is through the availability of enough oxygen.

The OH* images were recorded by using an Andor Solis iStar ICCD intensified camera. The camera is equipped with an UV objective with a 100 mm focal length f/2 lens and a 310 nm ± 10nm bandpass filter camera. The spatial resolution was 8.75 pixel/mm. For each injection one image was recorded. In this case, a sweep of 6 crank angle degrees was performed by using different delay times after the start of energizing (SOE). For each crank angle degree, 6 images were recorded.

2.5.3. 2-color pyrometry

2-color pyrometry is used in this work in order to quantify the soot concentration inside the piston bowl for each fuel tested. In this method, soot thermal radiation was detected for two specific wavelengths. From its combination, the soot surface temperature and optical density is determined [38]. In general, considering that the flame emits like a blackbody, the soot radiation intensity at a certain wavelength can be expressed by the Planck's law:

$$I_b(T,\lambda) = \frac{C_1}{\lambda^5\left[e^{\left(\frac{C_2}{\lambda T}\right)} - 1\right]} \qquad (1)$$

Where I_b is the radiance emitted by the blackbody. $C_1 = 1.1910439\ x\ 10^{-16} Wm^2/sr$ is the first Planck's constant, $C_2 = 1.4388\ X\ 10^{-2}\ mk$ is the second Planck's constant and λ is the wavelength. However, the flame (the soot) is a grey body with an emissivity ε below 1. Thus, the emission of the flame can be expressed as follows:

$$I(T,\lambda) = \varepsilon I_b(T,\lambda) \qquad (2)$$

By using the Hottel and Broughton (1932) empirical correlation[38], it is possible to express the emissivity as equation 3:

$$\varepsilon(KL,\lambda) = 1 - e^{-\left(KL_{2C}/\lambda^{\alpha}\right)} \qquad (3)$$

Where α is a parameter that depends on the soot properties (optical and physical). Zhao [38] reported that for the visible wavelength range, α=1.39 can be used for most fuels. KL_{2C} represents the dependence of emissivity with the amount of soot, and includes the total contribution of the soot along the optical path, no matter either soot distribution

or geometrical size[39]. Equation 2 can be applied for two measured wavelength, and temperature and KL_{2C} can be calculated.

For the current work, two Photron SA-5 high speed CMOS cameras were used. The flame radiation was splitted by using a beam splitter (50% transmission - 50% reflection). One of the cameras was equipped with an interference filter of 660 nm with 10 nm FWHM and another one with an interference filter of 550 nm with 10 nm FWHM as well. For both cameras, an objective with 100 mm focal length and f/2 was used. Images were recorded at 25 kfps with an exposure time of 6.65 µs for the 660 nm camera and 10.05 µs for the 550 nm camera. Calibration was performed by means of a tungsten-ribbon calibration lamp (Osram Wi17G) already used in previous studies[39][40]. The lamp was positioned just in the top piston squish zone (flat area), including in the calibration all optical devices used during the tests (mirrors, beam splitter and filters). For each condition, the cameras recorded 6 cycles of combustion.

2.6. Image post-processing

A specific methodology for the image analysis was developed in order to present time and spatially resolved KL_{2C} measurements in a single map. In this way, the combustion images were divided in zones by applying two different criteria: sector zones and radial zones. For the sector analysis, the whole piston image is divided in 5° angular sectors in the azimuth direction as shown in figure 4(a). For every sector an average KL is calculated.

For the radial analysis, the piston image is divided in rings, as shown in figure 4(b), with a difference of 0.5 mm between the internal and external radius. For each ring a mean

radius is calculated as well as the average KL_{2C}. The equations presented below are used for the two zone analysis

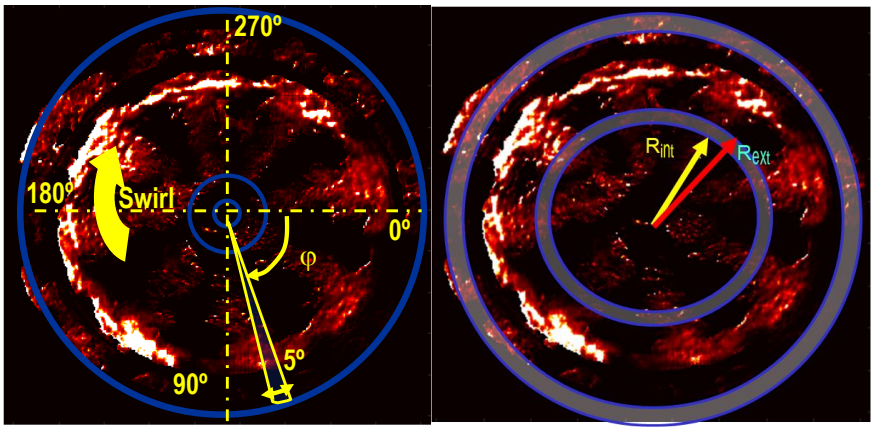

Figure 4. (a) methodology for the sector analysis. (b) methodology for the radial analysis

$$A_a = \sum_{i=pix,a} i \tag{4}$$

$$KL_{cummul,a} = \sum_{i=pix,a} KL_i \tag{5}$$

$$KL_{mean} = \frac{KL_{cummul,a}}{A_a} \tag{6}$$

Where the $A_a$is the soot area or the total amount of pixel identified as soot, present at each sector or ring region. $KL_{cummul,a}$ is the accumulated KL or the sum of all soot pixel values presented in the region considered (sector or radial). From the soot area A_a and $KL_{cummul,a}$, the mean KL value for each region is obtained.

2.7. In-cylinder pressure analysis

The heat release rate (HRR) was calculated by using the measured in-cylinder pressure. The in-cylinder pressure was measured for 15 consecutive combustion cycles. This is the maximum number of cycles that is possible to measure in the optical engine without the

need to stop and clean the optical accesses. A thermodynamic analysis is performed, by means of an in-house developed tool [41][42] in order to get the HRR. It is a one zone model and applies the first law of thermodynamic between the intake valve closing and exhaust valve opening. It takes into account heat transfer, blow-by and mechanical deformations. They were characterized in detail for this engine by Pastor et al [43]. From the HRR, it is possible to obtain the combustion phasing parameter used in this work, which is defined as the crank angle position where 50% of mass fraction has been burned (CA50). Furthermore, the combustion duration can be calculated as the difference between CA90 (90% of fuel burned) and CA5 (5% of fuel burned).

3. Results and discussion

In this section will be presented the main results found for each fuel applying the three different optical techniques. The discussion of results will be performed in detail for the condition at 7.5 bar of IMEP, where the images and results will be commented and compared with reports from the literature. For the other two conditions (1.5 and 4.5 bar of IMEP) the main results will be summarized at the end of this section.

3.1. Injection rate measurements

In figure 5 the injection rate measurement for each fuel is presented, corresponding to the 7.5 bar IMEP operating condition. The pilot 1 has different ET for fossil diesel than for FT diesel and OME_X, in order to get a similar CA50 and a similar HRR curve for the three fuels. SOE for the FT diesel and OME_X was delayed in relation to the fossil diesel in order to compensate for the different reactivity of the fuels. In the case of the pilot 2, SOE for the three fuels is almost the same, with a slight delay for the fossil diesel. For the main injection, the SOE was kept the same for all three fuels tested. FT diesel needs

a shorter ET than fossil diesel so the injected mass was slightly lower in order to guarantee the same IMEP. Although the FT diesel injected mass has been higher than fossil diesel, the injector behavior seems to be very similar. In relation to OME_X, besides the larger ET required for the OME_X (two times the one used for the other fuels) due to the lower LHV, the injector shows a different behavior. More specifically, it can be observed in figure 5 that it takes much more time for the injector to close once the ET has finished. The higher density and lower viscosity in comparison with to the other two fuels could be linked with this different behavior. Considering that the same dwell time was used for the three fuels between the end of the main injection and the start of the post injection energizing, in case of OME_X the two injections (main and post) seems to happen immediately one after another. This behavior was confirmed in the sequence of NL images as well. For the post injection, a similar phenomenon can be observed for the OME_X. After the energizing of the injector ends, it seems to be opened more time than for the other two fuels.

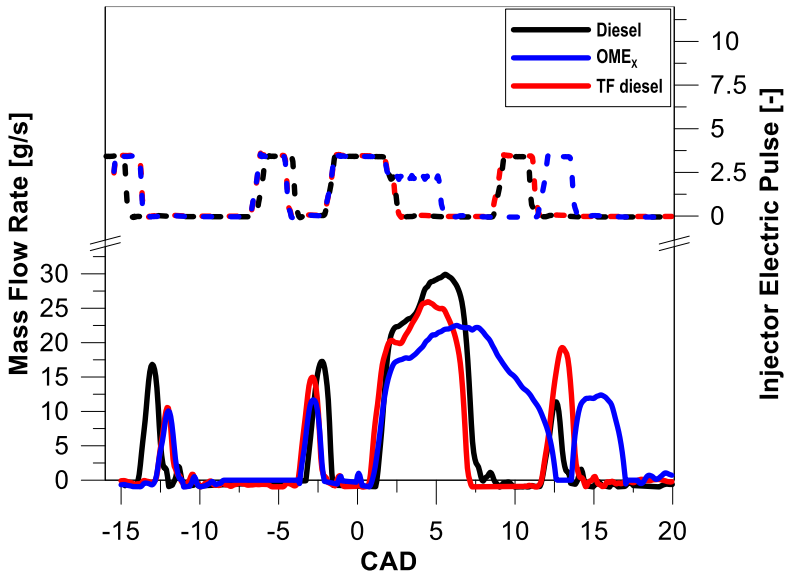

Figure 5.Mass flow rate and injector electric pulse at 7.5 bar of IMEP

3.2. Heat release and Natural Luminosity analysis

The Heat Release Rate and combustion evolution for specific crank angle degrees at 7.5 bar IMEP are presented in figures 6 and 7 respectively. It must be highlighted that the range of the natural luminosity intensity displayed for each fuel is different. For the OME_X, the maximum light intensity is around 400 while for FT and commercial diesel it reaches 2500. In fact, for OME_X test interference filter in front of the camera had to be removed to be able to register any radiation signal. This suggests less soot formation, which will be discussed in detail in the next sections.

First of all, looking at the HRR curve, it is possible to see that pilot 1 and 2 injections for the OME_X and FT diesel start to burn earlier even if the injection event occurred later. It is justified by the higher cetane number of both fuels in comparison with commercial diesel. However, the energy released from the OME_X during this stage of the cycle is lower than for the other two, due to the lower LHV. At -1.6 CAD, pilot 2 combustion has started as it is shown by the HRR curve of both OME_X and FT diesel. However, the commercial diesel is slightly delayed. At this point, radiation is still weak and is almost not observable for any of the three fuels.

From 4 CAD until 6.1 CAD, the main injection is taking place and the HRR curve rising is similar for the three fuels. FT diesel and fossil diesel seem to present the same combustion behavior as no significant difference in terms of radiation intensity can be perceived. In contrast, as it was indicated in the previous paragraphs, the OME_X combustion releases considerably less radiation than the other two. Besides, luminosity distribution is more uniform in this case, than for the other two fuels. It has been reported previously [24] that the lower OME_X viscosity causes a better atomization process, which improves air/fuel mixture. As a consequence, formation of rich zones is

reduced which directly avoids locally high soot formation. The high oxygen content in the fuel molecule acts in the same way, improving oxygen/carbon ratio in the combustion chamber.

At 9 CAD, the image of the commercial diesel presents some dark regions inside the piston bowl. Some authors have reported in previous works that at these regions, close to the bowl wall, the soot must be cold[44]. However, this is not observable for the FT diesel, suggesting the presence of hotter soot. This will be analyzed in more detail in the following sections. While the commercial diesel and FT diesel have already finished the main injection, OME_X is still injecting due to the larger ET, which is visible when comparing the HRR curves.

From 13.5 CAD until 25 CAD, the images are representing the post injection event and the late-cycle soot oxidation for the 3 fuels. FT diesel seems to oxidize faster than fossil diesel as the NL intensity decreases faster.

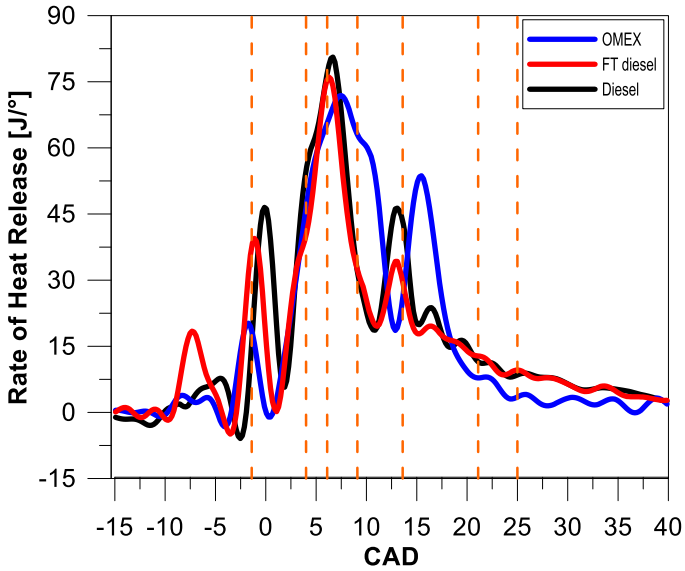

Figure 6. HRR diagram for each fuel at 7.5 bar IMEP

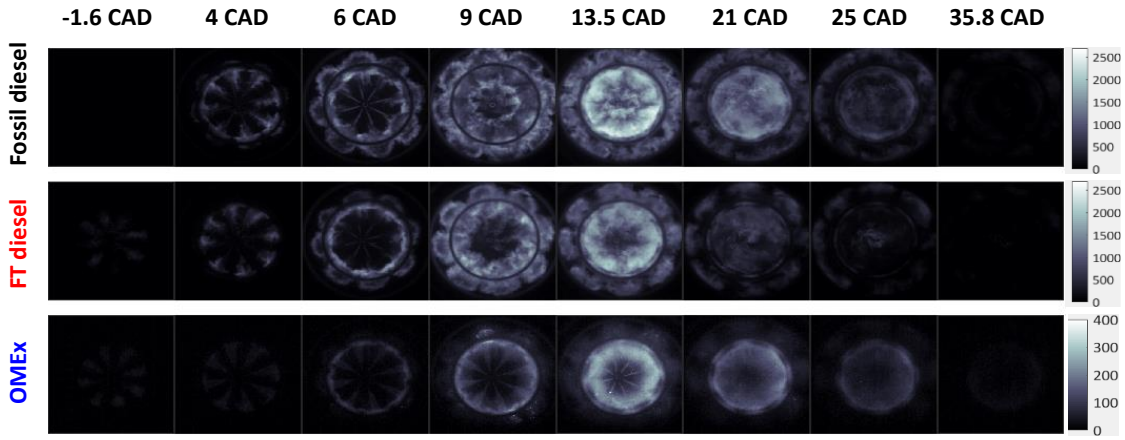

Figure 7. NL images of the combustion evolution for different crank angle degrees and fuels at 7.5 bar IMEP

The overall behavior each fuel is represented in figure 8. The accumulated NL intensity for the three fuels corresponding to 7.5 bar IMEP is shown. It confirms that OME_X emits less radiation than the other two fuels. Furthermore, the faster oxidation of the FT diesel in comparison with commercial diesel is also represented. Despite the largest injection duration for OME_X, the HRR curve and the NL confirms that its combustion duration is shorter.

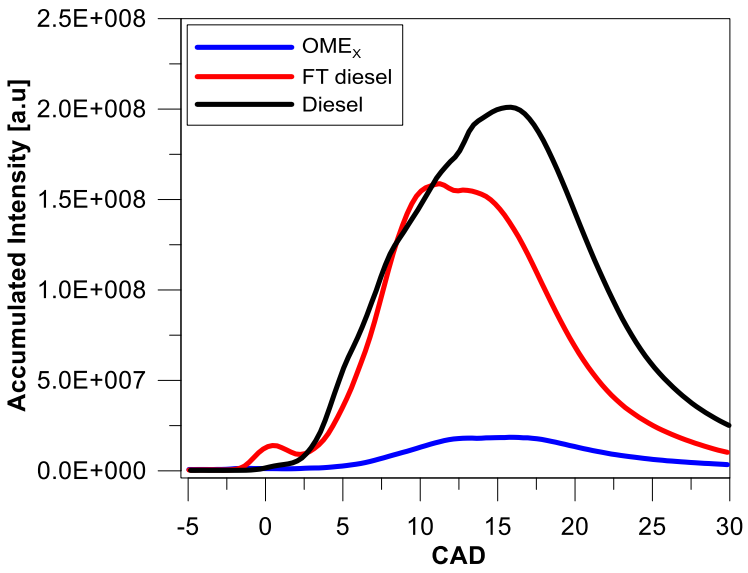

Figure 8. Accumulated intensity for each fuel at 7.5 bar IMEP

3.3. OH* chemiluminescence analysis

In figure 9, the OH* chemiluminescence for the three fuels is shown. Measurements were performed for six crank angle degrees and correspond to 7.5 bar IMEP. At -1.6 CAD no natural luminosity was observed. However, some OH* radiation is detected. This image is representing the pilot 2 combustion. Higher OH* chemiluminescence can be seen for the FT diesel during this period. It is coherent with the HRR curve (figure 6), where the peak for the FT diesel is higher. Moving forward in the cycle, at 4 CAD both NL and OH*images show high signal intensity in the periphery of the bowl for the 3 fuels. This result indicates that in this area both fuel rich and near-stoichiometric zones coexist, as found in previous works[37]. This evidences the importance of OH* in the soot oxidation process[45].

However, at 9 CAD differences between the OH* and NL images arise. The dark zones pointed out previously for the commercial diesel NL images correspond also to low OH* radiation. Taking into account that this radical in its exited state is present only in high temperature reaction zones, where the fuel/air ratio is near of stoichiometric, the lack of signal observed in this region could indicate the presence of rich fuel zones with soot at lower temperatures. At 13 CAD, it is possible to see that high OH* intensity appears again at the same area, as a result of the soot oxidation forced by the post injection.

When comparing the three fuels, at 9 CAD commercial diesel presents less area with OH* radiation than the FT diesel and consequently larger dark zones in the NL images. In addition, although OME_X presented the lowest NL intensity, the OH* measurements show the highest intensity. As it has been mentioned previously, the high amount of oxygen in the OME_X and its better fuel atomization due to the low viscosity, reduces the

fuel rich local zones and increases the near-stoichiometric zones as well as the presence of OH* in excited state.

At the final stages of combustion (35.8 CAD) the OH* signal confirms that, despite OME_X having a longer injection duration, the combustion ends earlier as almost no OH* signal is observed in comparison with the other two fuels. Furthermore, fossil diesel has the higher OH* intensity for this instant, indicating a slower soot oxidation process in comparison with the FT diesel.

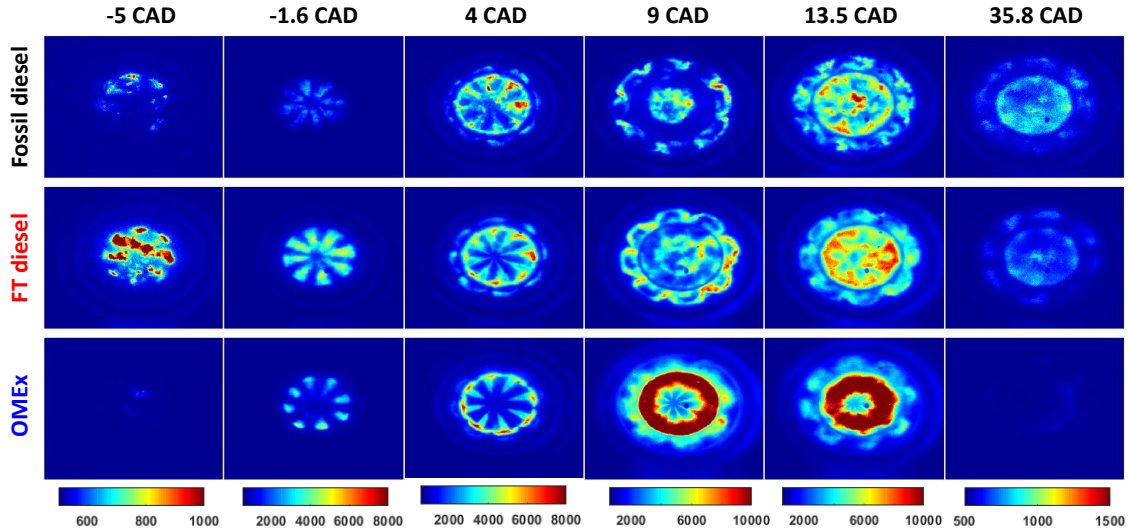

Figure 9.OH* chemiluminescence images for different crank angle degrees and fuels at 7.5 bar IMEP

3.4. 2-color pyrometry

The soot measurement at 7.5 bar IMEP was obtained by means of the2-color pyrometry technique. Taking into account that the flame radiation emitted by the OME_X was below the threshold of the camera detection when the interference filter was in place, measurements were possible only for the FT diesel and commercial diesel. In figure 10, the same piston positions presented previously for the NL and OH* images are also shown for the 2 color-pyrometry images. The color scale corresponds to the soot KL_{2C} parameter, which is an indicator of soot concentration.

From -1.6 CAD until 1.6 CAD the KL_{2C} is almost unmeasurable due to the weak radiation detected. From 4 CAD until 6 CAD, during the main injection, the soot concentration (KL_{2C}) starts to increase. The highest soot areas are localized in the bowl periphery where the NL and OH* showed highest intensity. Until 6 CAD there is no significant difference between FT diesel and commercial diesel. At 9 CAD, the region where NL and OH* signals for commercial diesel were weak corresponds to the highest soot volume fraction region measured with 2 color. For this instant, FT diesel presents KL_{2C} values slightly lower than commercial diesel, which means less soot production. The larger differences can be found for this instant in the squish zone.

From 13.5 CAD to 25 CAD, after the post-injection, the KL_{2C} images and NL images have a good agreement. Areas with high light intensity in the NL images correspond to areas with high KL_{2C}. In addition, FT diesel still shows lower KL_{2C} values than commercial diesel.

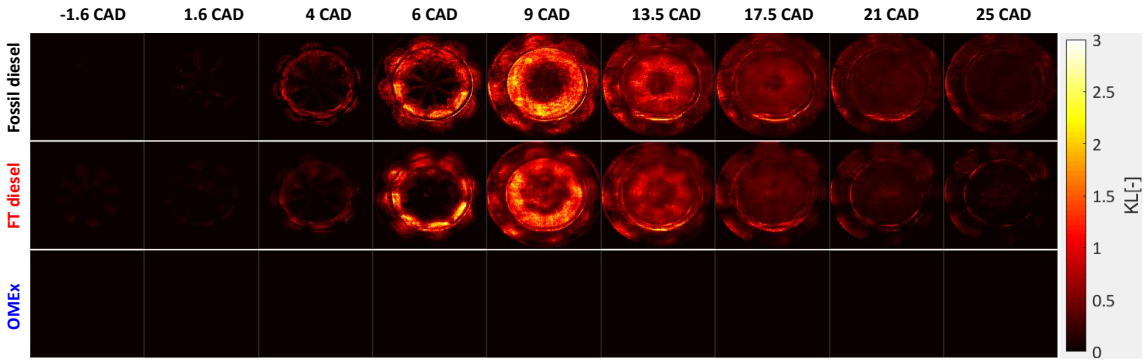

Figure 10. Soot volume fraction inside combustion chamber for different crank angle degrees and fuels at 7.5 bar IMEP

The soot evolution is summarized in figure 11. Curves of average KL are shown for the three fuels. As discussed previously, OME_X was below the detection threshold of the optical system. As it can be observed, commercial diesel starts to increase earlier in the cycle than FT diesel. Furthermore, it is clear that for the first one, the maximum KL value

is slightly higher. In addition, during the oxidation process, FT diesel seems to oxidize faster, in agreement with NL and OH* observations.

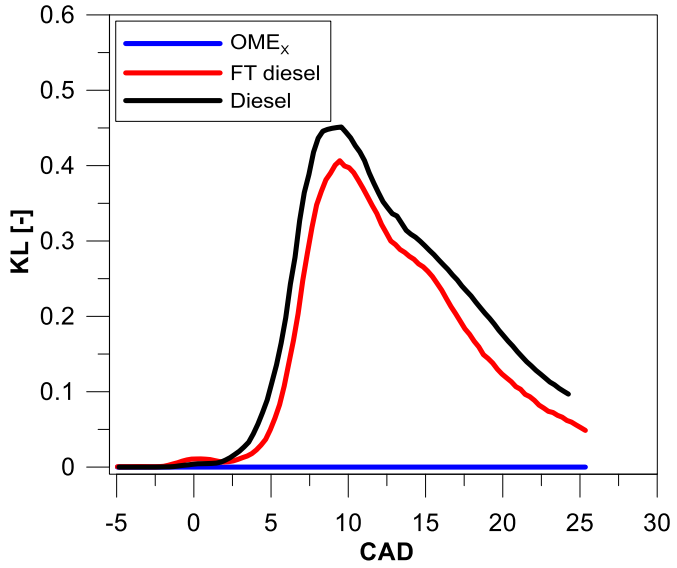

Figure 11. Mean KL evolution at 7.5 bar IMEP

In figure 12 the maps based on sector and radial discretization are represented. They represent spatial resolution in the y-axis and temporal resolution in the x-axis. For the sectors map (figure 12 - left) the pink lines correspond to the spray axes. Thus, separating the combustion chamber in small sectors enable to visualize and analyze how is the combustion evolution for each spray.

The first thing that can be noticed for both fuels is the non-uniformity of the soot production for each spray. This effect could be related with some uncertainties in the experiments such as the non-homogeneous temperature distribution inside the cylinder or the different behavior of injector holes due to carbon deposition. Furthermore, although the maps for each fuel are similar, they evidence that the higher soot formation for the commercial diesel is not concentrated in a specific region but along the whole combustion chamber. When analyzing spray by spray, it is possible to see that commercial diesel present larger areas with high KL values than FT diesel. Furthermore,

from the map is possible to see that the FT diesel achieves lower KL values before than commercial diesel due to the less soot generated inside the cylinder and the faster oxidation.

The radial maps (figure 12 – right) help to understand where highest soot concentrations are located and, furthermore, to visualize how soot evolves inside the bowl while the combustion process is occurring. Initially, the highest soot KL is located in the periphery of the bowl at around 15 mm from the injector. As the piston moves far from the TDC, the highest soot KL areas move toward the center of the piston while decreasing its value. However small differences can be identified between the two fuels. FT diesel achieves low KL (below 0.5) at around of 6mm of radius, while commercial diesel reaches these values closer to bowl center. It evidences again the faster soot oxidation for the FT diesel. Another difference is located in the squish zone, which comprehends from 18mm to 26 mm. For this region, the soot concentration is lower for the FT diesel.

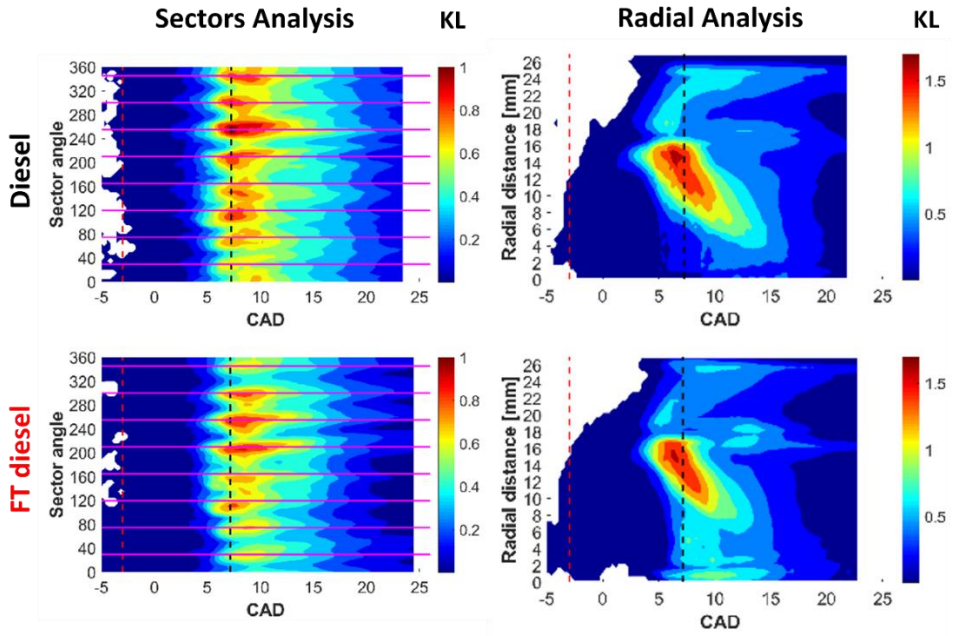

Figure 12. Spatial and temporal soot volume fraction distribution for FT diesel and fossil diesel at 7.5 bar IMEP for sectors and radial analysis

3.5. 4.5 bar and 1.5 bar IMEP analysis

The same sequence of tests and methodology was applied for other two conditions, 4.5 and 1.5 bar IMEP. In figure 13, the accumulated intensity from the NL measurements for the three fuels and the two conditions is shown. It can be seen that OME_X, as it was described previously, presents the lowest radiation values for both conditions tested. In addition, at 1.5 bar IMEP, accumulated intensity curve for the commercial diesel is higher than for FT diesel as it was already seen for 7.5 IMEP. However, a different trend is noted at 4.5 bar. In this case, the peak of accumulated intensity for FT diesel is slightly higher than for the commercial diesel. The high quantity of cold soot at 4.5 bar IMEP for diesel could be the responsible of the weaker natural luminosity detected. A region of cold soot emits low-intensity radiation but absorbs large amounts of light. This is represented by the dark regions which are formed during the combustion process. They diminish the accumulated luminosity as shown in figure 13. At 4.5 bar IMEP this phenomena is more relevant than at 7.5 bar IMEP due to the lower injection pressure, which contributes to the formation of rich fuel zones.

In figure 14, it is possible to see that this behavior is not followed by the KL measurements. The mean KL curve at 4.5 bar is indicating a higher soot production for the commercial diesel, as it was observed for the other operating conditions. This points out the limitations of soot formation analysis based only on natural luminosity measurements and the benefits of an additional technique like 2-color pyrometry.

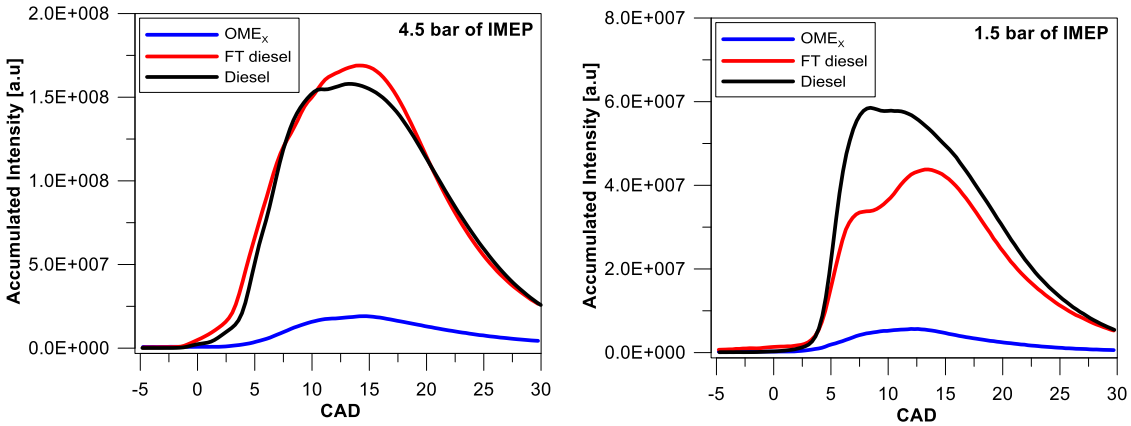

Figure 13 Accumulate intensity for (a) 4.5 bar and (b) 1.5 bar of IMEP

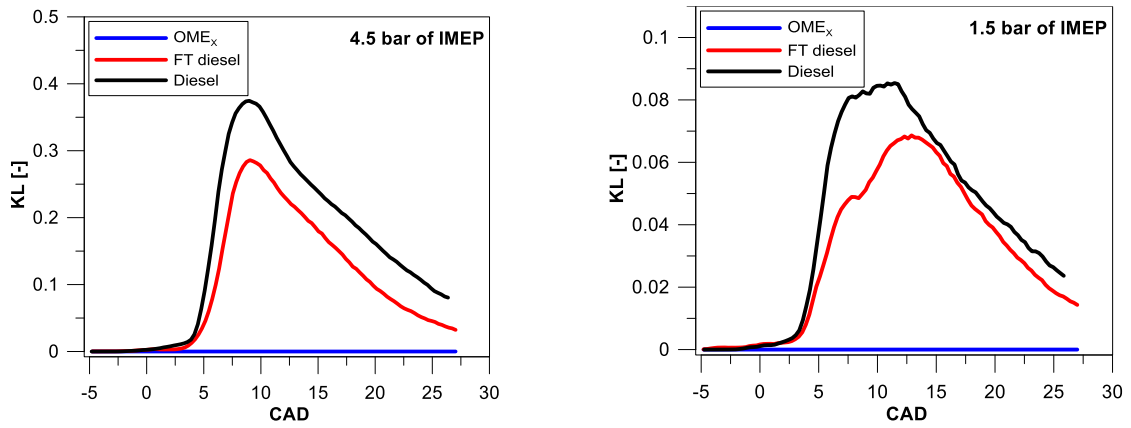

Figure 14 Mean KL evolution for (a) 4.5 bar and (b) 1.5 bar of IMEP

4. Conclusions

The current paper has evaluated the combustion process and soot formation of two different E-fuels by using three different optical techniques. The results were compared with the commercial diesel and the main conclusions for each technique used are presented below.

Considering the Heat Release Rate and Natural Luminosity images:

- The pilot 1 evidences the higher cetane number of FT diesel. Although the pilot 1 is delayed for the FT diesel in relation to the commercial diesel, the combustion is starting earlier.

- Although OME_X has a larger main injection duration than the other two fuels, HRR curve is indicating that the combustion ends earlier.

- OME_X presented a much lower light intensity than FT diesel and commercial diesel for the three conditions tested, reinforcing the idea that it is a non-sooting fuel.

- In terms of maximum light intensity, FT diesel has showed lower values than diesel. However, dark regions were observed for the commercial diesel which are related with high concentration of cold soot.

- FT diesel light intensity reduces faster than commercial diesel, indicating that the soot oxidation seems to finish earlier.

In relation to the OH* chemiluminescence images:

- The highest peak for the FT diesel in the HRR curve during the pilot 1 is confirmed by the OH* images, where the intensity is higher as well.

- The dark zones, which were visualized previously in the NL images at 9.1 CAD, in the OH* measurements are represented by the ring with low intensity. This is due to the high concentration of soot is blocking the OH* chemiluminescence signal or there is no chemical reaction occurring in this zone. In this case, the OH* intensity signal of FT diesel is higher than commercial diesel.

- Although the NL intensity for the OME_X is lowest between the three fuels, it presents the highest OH* intensity. The high amount of oxygen can increase the local zones near of stoichiometric conditions and increases the OH* intensity. Furthermore, the very low soot formation permits a better visualization of the OH*

chemiluminescence that is not possible to see for the case with FT diesel and fossil diesel.

- The images at 35.8 CAD prove the shortest combustion duration for the OME_X. Furthermore, it is clear that FT diesel presents a faster oxidation than commercial diesel.

Finally, applying 2 color pyrometry is possible to state:

- FT diesel presents lower soot emissions than commercial diesel for the three conditions tested.
- At 9 CAD, the dark zones in the NL images correspond to the highest soot concentration zones in the 2 color images.
- Faster oxidation for the FT diesel in relation to the commercial diesel is evidenced again in the 2 color technique.
- No correlation of NL images and 2 color images at 9 CAD. Dark zones (low intensity) in NL images represents high soot concentration in 2 color images. From 13.5 until 25 CAD, the highest NL intensity corroborates with the highest KL values.
- Radial map presents lower KL values in the squish zone when FT diesel was used. Furthermore, the FT diesel flame oxidize the soot farther from the center than commercial diesel.

Acknowledgments

This work was partially funded by Generalitat Valenciana through the Programa Santiago Grisolía (GRISOLIAP/2018/142) program.

References

[1] J. Benajes, A. García, J. Monsalve-Serrano, R. Lago Sari, Fuel consumption and engine-out emissions estimations of a light-duty engine running in dual-mode RCCI/CDC with different fuels and driving cycles, Energy. 157 (2018) 19–30. doi:10.1016/j.energy.2018.05.144.

[2] N. Dronniou, J. Kashdan, B. Lecointe, K. Sauve, D. Soleri, Optical Investigation of Dual-fuel CNG/Diesel Combustion Strategies to Reduce CO2 Emissions, SAE Int. J. Engines. 7 (2014) 873–887. doi:10.4271/2014-01-1313.

[3] C. Geng, H. Liu, B. Chen, M. Yao, X. Ran, Z. Yang, L. Feng, Q. Tang, A comparative study on partially premixed combustion (PPC) and reactivity controlled compression ignition (RCCI) in an optical engine, Proc. Combust. Inst. 37 (2018) 4759–4766. doi:10.1016/j.proci.2018.06.004.

[4] S. Tanov, B. Johansson, M. Richter, Z. Wang, H. Wang, Effects of Injection Strategies on Fluid Flow and Turbulence in Partially Premixed Combustion (PPC) in a Light Duty Engine, SAE Tech. Pap. Ser. 1 (2015). doi:10.4271/2015-24-2455.

[5] A. Matamis, M. Richter, M. Tuner, M.O. Lundgren, O. Andersson, A. Arne, Z. Wang, M. Alden, Effects of Post-Injections Strategies on UHC and CO at Gasoline PPC Conditions in a Heavy-Duty Optical Engine, SAE Tech. Pap. Ser. 1 (2017). doi:10.4271/2017-01-0753.

[6] S. Busch, K. Zha, E. Kurtz, A. Warey, R. Peterson, Experimental and Numerical Studies of Bowl Geometry Impacts on Thermal Efficiency in a Light-Duty Diesel Engine, SAE Tech. Pap. Ser. 1 (2018) 1–12. doi:10.4271/2018-01-0228.

[7] K. Zha, S. Busch, A. Warey, R.C. Peterson, E. Kurtz, A Study of Piston Geometry Effects on Late-Stage Combustion in a Light-Duty Optical Diesel Engine Using Combustion Image Velocimetry, SAE Int. J. Engines. 11 (2018) 783–804. doi:10.4271/2018-01-0230.

[8] A. Omari, B. Heuser, S. Pischinger, C. Rüdinger, Potential of long-chain oxymethylene ether and oxymethylene ether-diesel blends for ultra-low emission engines, Appl. Energy. 239 (2019) 1242–1249. doi:10.1016/j.apenergy.2019.02.035.

[9] S. Siegemund, M. Trommler, O. Kolb, V. Zinnecker, P. Schmidt, W. Weindorf, W. Zittel, T. Raksha, J. Zerhusen, E-Fuels study. The potential of electricity-based fuels for low-emission transport in the EU, Dtsch. Energie-Agentur GmbH. (2017).

[10] B. Hao, C. Song, G. Lv, B. Li, X. Liu, K. Wang, Y. Liu, Evaluation of the reduction in carbonyl emissions from a diesel engine using Fischer-Tropsch fuel synthesized from coal, Fuel. 133 (2014) 115–122. doi:10.1016/j.fuel.2014.05.025.

[11] S. Kook, L.M. Pickett, Liquid length and vapor penetration of conventional, Fischer-Tropsch, coal-derived, and surrogate fuel sprays at high-temperature and high-pressure ambient conditions, Fuel. 93 (2012) 539–548. doi:10.1016/j.fuel.2011.10.004.

[12] A. Rimkus, J. Žaglinskis, P. Rapalis, P. Skačkauskas, Research on the combustion, energy and emission parameters of diesel fuel and a biomass-to-liquid (BTL) fuel blend in a compression-ignition engine, Energy Convers. Manag. 106 (2015) 1109–1117. doi:10.1016/j.enconman.2015.10.047.

[13] S. Schemme, R.C. Samsun, R. Peters, D. Stolten, Power-to-fuel as a key to sustainable transport systems – An analysis of diesel fuels produced from CO 2 and renewable electricity, Fuel. 205 (2017) 198–221. doi:10.1016/j.fuel.2017.05.061.

[14] M. Lapuerta, O. Armas, J.J. Hernández, A. Tsolakis, Potential for reducing emissions in a diesel engine by fuelling with conventional biodiesel and Fischer-Tropsch diesel, Fuel. 89 (2010) 3106–3113. doi:10.1016/j.fuel.2010.05.013.

[15] S.S. Gill, A. Tsolakis, K.D. Dearn, J. Rodríguez-Fernández, Combustion characteristics and emissions of Fischer–Tropsch diesel fuels in IC engines, Prog. Energy Combust. Sci. 37 (2011) 503–523. doi:10.1016/J.PECS.2010.09.001.

[16] Y. Jiao, R. Liu, Z. Zhang, C. Yang, G. Zhou, S. Dong, W. Liu, Comparison of combustion and emission characteristics of a diesel engine fueled with diesel and methanol-Fischer-Tropsch diesel-biodiesel-diesel blends at various altitudes, Fuel. 243 (2019) 52–59. doi:10.1016/j.fuel.2019.01.107.

[17] A. Abu-Jrai, A. Tsolakis, K. Theinnoi, R. Cracknell, A. Megaritis, M.L. Wyszynski, S.E. Golunski, Effect of gas-to-liquid diesel fuels on combustion characteristics, engine emissions, and exhaust gas fuel reforming. Comparative study, Energy and Fuels. 20 (2006) 2377–2384. doi:10.1021/ef060332a.

[18] P. Rounce, A. Tsolakis, J. Rodríguez-Fernández, A.P.E. York, R.F. Cracknell, R.H. Clark, Diesel Engine Performance and Emissions when First Generation Meets Next Generation Biodiesel, SAE Tech. Pap. Ser. 1 (2010) 1–10. doi:10.4271/2009-01-1935.

[19] P. Schaberg, J. Botha, M. Schnell, H.O. Hermann, N. Pelz, R. Maly, Emissions performance of GTL diesel fuel and blends with optimized engine calibrations, SAE Tech. Pap. (2005). doi:10.4271/2005-01-2187.

[20] S.E. Iannuzzi, C. Barro, K. Boulouchos, J. Burger, Combustion behavior and soot formation/oxidation of oxygenated fuels in a cylindrical constant volume chamber, Fuel. 167 (2016) 49–59. doi:10.1016/j.fuel.2015.11.060.

[21] L. Pellegrini, M. Marchionna, R. Patrini, C. Beatrice, N. Del Giacomo, C. Guido, Combustion Behaviour and Emission Performance of Neat and Blended Polyoxymethylene Dimethyl Ethers in a Light-Duty Diesel Engine, SAE Tech. Pap. Ser. 1 (2012). doi:10.4271/2012-01-1053.

[22] R. Zhu, X. Wang, H. Miao, Z. Huang, J. Gao, D. Jiang, Performance and Emission Characteristics of Diesel Engines Fueled with Diesel−Dimethoxymethane (DMM) Blends, Energy & Fuels. 23 (2009) 286–293.

[23] M. Härtl, P. Seidenspinner, E. Jacob, G. Wachtmeister, Oxygenate screening on a heavy-duty diesel engine and emission characteristics of highly oxygenated oxymethylene ether fuel OME1, Fuel. 153 (2015) 328–335. doi:10.1016/j.fuel.2015.03.012.

[24] H. Liu, Z. Wang, Y. Li, Y. Zheng, T. He, J. Wang, Recent progress in the application in compression ignition engines and the synthesis technologies of polyoxymethylene dimethyl ethers, Appl. Energy. 233–234 (2019) 599–611. doi:10.1016/j.apenergy.2018.10.064.

[25] A. Omari, B. Heuser, S. Pischinger, Potential of oxymethylenether-diesel blends

for ultra-low emission engines, Fuel. 209 (2017) 232–237. doi:10.1016/j.fuel.2017.07.107.

[26] X. Ma, Y. Ma, S. Sun, S.-J. Shuai, Z. Wang, J.-X. Wang, PLII-LEM and OH* Chemiluminescence Study on Soot Formation in Spray Combustion of PODEn-Diesel Blend Fuels in a Constant Volume Vessel, SAE Tech. Pap. Ser. 1 (2017). doi:10.4271/2017-01-2329.

[27] H. Liu, Z. Wang, J. Zhang, J. Wang, S. Shuai, Study on combustion and emission characteristics of Polyoxymethylene Dimethyl Ethers/diesel blends in light-duty and heavy-duty diesel engines, Appl. Energy. 185 (2017) 1393–1402. doi:10.1016/j.apenergy.2015.10.183.

[28] B. Lumpp, D. Rothe, C. Pastötter, R. Lämmermann, E. Jacob, OXYMETHYLENE ETHERS AS DIESEL FUEL ADDITIVES OF THE FUTURE, MTZ Worldw. EMagazine. 72 (2011) 34–38. doi:10.1365/s38313-011-0027-z.

[29] H. Liu, Z. Wang, J. Wang, X. He, Improvement of emission characteristics and thermal efficiency in diesel engines by fueling gasoline/diesel/PODEn blends, Energy. 97 (2016) 105–112. doi:10.1016/j.energy.2015.12.110.

[30] H. Chen, X. Su, J. Li, X. Zhong, Effects of gasoline and polyoxymethylene dimethyl ethers blending in diesel on the combustion and emission of a common rail diesel engine, Energy. 171 (2019) 981–999. doi:10.1016/j.energy.2019.01.089.

[31] R. Payri, J. De La Morena, J. Monsalve-Serrano, F.C. Pesce, A. Vassallo, Impact of counter-bore nozzle on the combustion process and exhaust emissions for light-duty diesel engine application, Int. J. Engine Res. 20 (2019) 46–57.

doi:10.1177/1468087418819250.

[32] S.H. Park, H.J. Kim, C.S. Lee, Effect of Multiple Injection Strategies on Combustion and Emission Characteristics in a Diesel Engine, Energy and Fuels. 30 (2016) 810–818. doi:10.1021/acs.energyfuels.5b02121.

[33] L. De Simio, S. Iannaccone, Gaseous and particle emissions in low-temperature combustion diesel–HCNG dual-fuel operation with double pilot injection, Appl. Energy. 253 (2019) 113602. doi:10.1016/j.apenergy.2019.113602.

[34] M. Denny, F. Holst, A. Helmantel, H. Persson, P. Tunestål, Ö. Andersson, Impact of closely-coupled triple-pilot and conventional double-pilot injection strategies in a LD diesel engine, Fuel. 246 (2019) 141–148. doi:10.1016/j.fuel.2019.02.101.

[35] J. V. Pastor, J.M. García-Oliver, A. García, M. Pinotti, Laser induced plasma methodology for ignition control in direct injection sprays, Energy Convers. Manag. 120 (2016) 144–156. doi:10.1016/j.enconman.2016.04.086.

[36] C.J. Mueller, G.C. Martin, Effects of Oxygenated Compounds on Combustion and Soot Evolution in a DI Diesel Engine:Broadband Natural Luminosity Imaging, SAE Tech. Pap. Ser. 1 (2010). doi:10.4271/2002-01-1631.

[37] M. Jakob, T. Hülser, A. Janssen, P. Adomeit, S. Pischinger, G. Grünefeld, Simultaneous high-speed visualization of soot luminosity and OH * chemiluminescence of alternative-fuel combustion in a HSDI diesel engine under realistic operating conditions, Combust. Flame. 159 (2012) 2516–2529. doi:10.1016/j.combustflame.2012.03.004.

[38] H. Zhao, Laser Diagnostics and Optical Measurement Techniques in Internal

Combustion Engines, SAE International, 2012.

[39] J. V. Pastor, A. García, C. Micó, S. Möller, J.M. García-Oliver, Application of optical diagnostics to the quantification of soot in n -alkane flames under diesel conditions, Combust. Flame. 164 (2015) 212–223. doi:10.1016/j.combustflame.2015.11.018.

[40] T. Xuan, J. V. Pastor, J.M. García-Oliver, A. García, Z. He, Q. Wang, M. Reyes, In-flame soot quantification of diesel sprays under sooting/non-sooting critical conditions in an optical engine, Appl. Therm. Eng. 149 (2019) 1–10. doi:10.1016/j.applthermaleng.2018.11.112.

[41] F. Payri, S. Molina, J. Martín, O. Armas, Influence of measurement errors and estimated parameters on combustion diagnosis, Appl. Therm. Eng. 26 (2006) 226–236. doi:10.1016/j.applthermaleng.2005.05.006.

[42] F. Payri, P. Olmeda, J. Martín, A. García, A complete 0D thermodynamic predictive model for direct injection diesel engines, Appl. Energy. 88 (2011) 4632–4641. doi:10.1016/j.apenergy.2011.06.005.

[43] J. Pastor, P. Olmeda, J. Martín, F. Lewiski, Methodology for Optical Engine Characterization by Means of the Combination of Experimental and Modeling Techniques, Appl. Sci. 8 (2018) 2571. doi:10.3390/app8122571.

[44] G. Roberts, T. Lind, W. Eagle, M.P. Musculus, Ö. Andersson, C. Rousselle, Mechanisms of Post-Injection Soot-Reduction Revealed by Visible and Diffused Back-Illumination Soot Extinction Imaging, SAE Tech. Pap. Ser. 1 (2018) 1–20. doi:10.4271/2018-01-0232.

[45] H. Kosaka, T. Nishigaki, T. Kamimoto, T. Sano, A. Matsutani, S. Harada, Simultaneous 2-D Imaging of OH Radicals and Soot in a Diesel Flame by Laser Sheet Techniques, SAE Tech. Pap. Ser. 1 (2010). doi:10.4271/960834.

Nomenclature

NOx: Nitrogen Oxides

FT disel: Fischer-Tropsch diesel

PM: Particulate matter

CO: Carbon Monoxide

HC: Hydrocarbons

EGR: Exhaust Gas Recirculation

OME_X: Oxymethylene dimethyl ether

LHV: Lower Heating Value

ET: Energizing Time

IMEP: Indicated Mean Effective Pressure

SOE: Start of Energizing

CAD: Crank Angle Degree

UV: Ultraviolet

NL: Natural Luminosity

KL: Optical Thickness

HRR: Heat Release Rate

TDC: Top Dead Center

CI: Compression Ignition